

DISCOVERY OF WADALITE IN ALLENDE TYPE B CAI. H. A. Ishii¹, A. N. Krot², K. Keil², K. Nagashima², J. P. Bradley¹, N. Teslich¹, B. Jacobsen³ and Q. Z. Yin³, ¹Institute of Geophysics and Planetary Physics, Lawrence Livermore National Laboratory, Livermore, CA 94550, USA (hope.ishii@llnl.gov), ²Hawaii Institute of Geophysics and Planetology, University of Hawaii at Manoa, Honolulu, HI 96822, USA (sasha@higp.hawaii.edu), ³Department of Geology, University of California at Davis, Davis, CA 95616, USA.

Introduction: We present electron microprobe, SEM and FIB-TEM analyses on Allende Type B CAI fragments in which the Cl-bearing mineral wadalite has been identified for the first time in a meteoritic material. The ideal wadalite formula is $\text{Ca}_6\text{Al}_5[\text{O}_8(\text{SiO}_4)_2\text{Cl}_3]$ and, typically, it occurs as $\text{Ca}_6(\text{Al},\text{Si},\text{Fe},\text{Mg})_7\text{O}_{16}\text{Cl}_3$. In terrestrial occurrences, wadalite is found in skarns as a secondary product of retrogressive hydrothermal alteration of spurrite (a Ca-Si-carbonate) and gehlenite [1]. We propose an analogous mechanism involving interaction of Cl-bearing fluid with grossular for wadalite formation in CAIs.

Methods: Electron microprobe and scanning electron microscopy were initially carried out on polished fragments with a Cameca SX-50 and JEOL 5900LV SEM/EDS. Further imaging preparatory to FIB sectioning was carried out on a JEOL JSM-7401F SEM. Using an FEI Nova600 NanoLab dual-beam FIB, site-specific electron-transparent thin sections were extracted for subsequent TEM analysis on a 200kV FEI Tecnai TF20 G2 monochromated STEM.

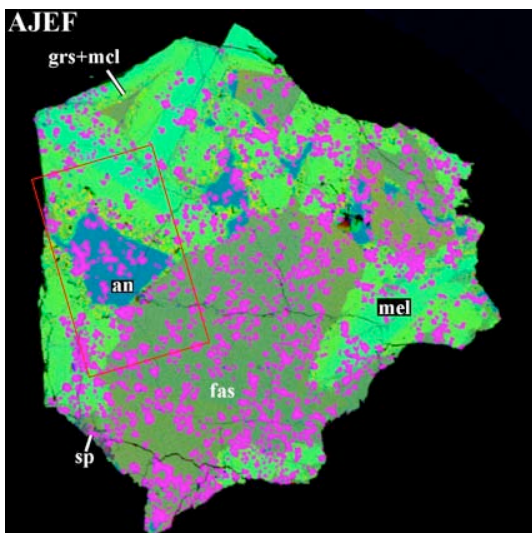


Figure 1. Combined elemental map of the Allende CAI AJEF (~2 mm) from Mg (red), Ca (green) and Al (blue) $K\alpha$ x-rays. Red box indicates region in Fig. 2. (an=anorthite, sp=spinel, fas=fassaite, mel=melilite, grs=grossular)

Overview mineralogy: Allende fragment AJEF is a coarse-grained Type B CAI composed of melilite, fassaite, spinel and minor anorthite (Fig. 1). Both melilite (Åk_{19-64}) and fassaite (2-11 wt% TiO_2 , 14-18 wt% Al_2O_3) display chemical zoning with enrichment in Na

accompanying increasing Åk content. Melilite is cross-cut by veins composed of grossular, monticellite, wollastonite and wadalite. Åk ermanitic melilite around anorthite and fassaite grains is more extensively replaced by these secondary minerals (Fig. 2) Secondary nepheline and sodalite are minor. Wadalite has been located in another Allende coarse-grained Type B CAI, fragment A39 where, in altered regions, enrichments in Na track depletions in Ca.

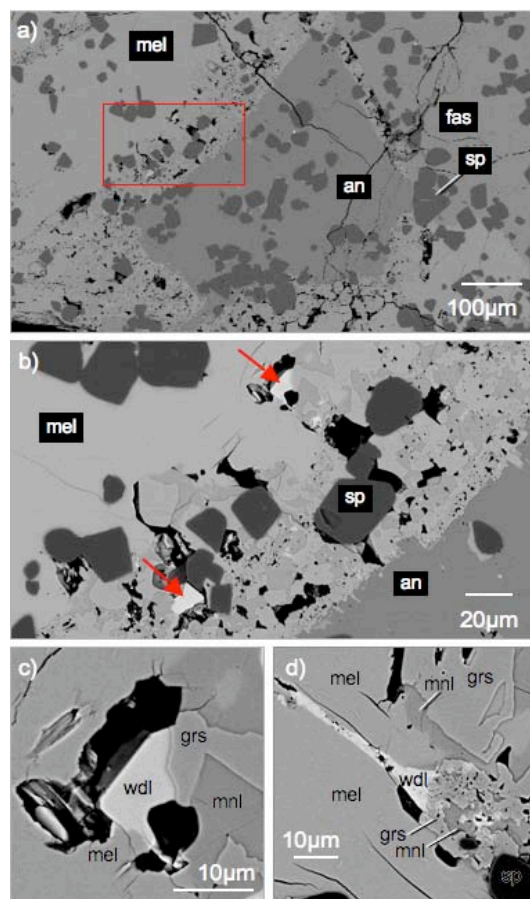


Figure 2. 10 kV backscattered electron images of Allende CAI AJEF. a) Low magnification image, b) area denoted by red box in a) with wadalite grains indicated by arrows and c) petrographic setting of a wadalite grain and d) a wadalite vein. (wdl=wadalite, mnl=monticellite)

Wadalite identification: Electron microprobe analyses of Cl-bearing grains in Allende Type B CAI fragments are consistent with literature values (Table 1). To confirm this preliminary identification, a FIB section crossing a grain (Fig. 2c) in a boundary region

with secondary minerals around an anorthite grain was extracted and thinned to electron transparency (Fig. 3) for TEM analysis. TEM selected area diffraction secures the identification of wadalite with a cubic I-43d lattice and $a_0=12.0\text{\AA}$ (Fig. 4). Diffraction patterns were internally calibrated by the polycrystalline Pt overcoat ($d_{111}=2.27\text{\AA}$).

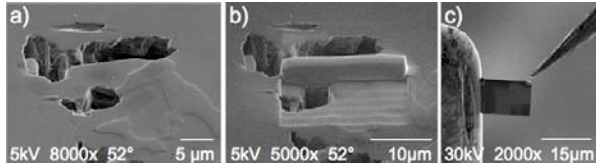


Figure 3. FIB sample preparation. SEM images of a) FIB section location (52° tilt relative to Fig 2c) and b) protective Pt strap and partially milled trench, and c) ion image of FIB section removed from AJEF and attached to TEM grid.

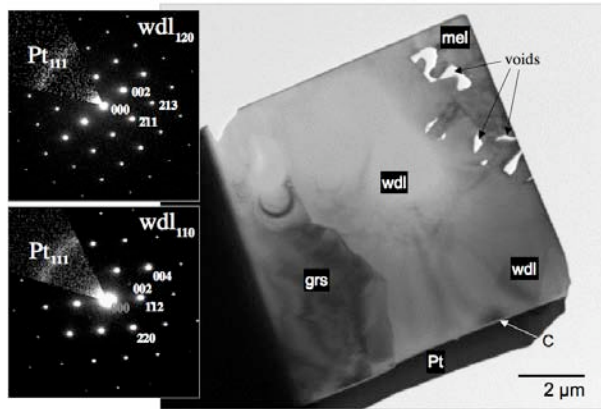


Figure 4. Bright field TEM image (right) of FIB section containing wadalite. Selected area diffraction patterns (left) along the $[120]$ and $[110]$ zones with Pt $[111]$ pattern inset.

Discussion: Wadalite in Allende CAIs is commonly found adjacent to melilite and its alteration products grossular and monticellite. Chemically, wadalite is most closely related to grossular, and it is found in AJEF both as discrete grains (Fig. 2c) and filling veins in melilite (Fig. 2d). Grossular-bearing assemblages lacking Cl- or Na-bearing minerals are also present indicating that wadalite formation occurred at relatively low temperatures after the secondary alteration that generated grossular. Interaction of grossular with a Cl-bearing fluid can account for wadalite grain formation as well as wadalite deposited by the fluid in existing cracks to form veins.

Anorthite (Fig. 2b) displays a coarsely-roughened interface at its surrounding $\sim 80\text{-}100\ \mu\text{m}$ wide rim of secondary minerals while fassaite does not. This may also be indicative of fluid phase chemistry giving rise to preferential dissolution/etching of anorthite.

In the FIB section, wadalite resides between grossular and melilite. The wadalite-grossular interface is smooth, but the interface between wadalite and melilite

is complex. Bright field TEM images (Fig. 5) show melilite laths that seem to intersect the wadalite in voids. Melilite in the FIB section is $\sim \text{\AA}k_{12}$, a lower $\text{\AA}k$ content than the bulk melilite suggesting these melilite laths may have recrystallized during the fluid-mediated alteration that produced wadalite. The void structures may also be the vestiges of fluid inclusions.

An assessment of the crystallographic relationships between wadalite, melilite and grossular will aid in understanding the mechanisms by which wadalite formed and where in the sequence of secondary alterations it resides. Results from additional FIB-TEM sections through wadalite-containing regions will be discussed.

Conclusions: We have positively identified wadalite for the first time in meteoritic materials, specifically, in Allende CAIs. Based on petrographic details, wadalite in the Allende Type B CAIs most likely formed by interaction of grossular with a Cl-bearing fluid at modest temperature and pressure.

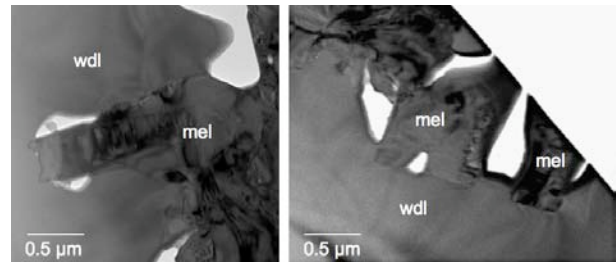


Figure 5. Bright field TEM images of the wadalite-melilite interface with melilite laths across void spaces.

wt%	Ref [1]	wdl-1	wdl-2	wdl-3
CaO	41.1	40.8	41.5	40.8
MgO	3.1	4.9	3.3	4.2
Al ₂ O ₃	20.9	18.3	22.1	20.5
SiO ₂	19.8	24.8	20.1	22.2
Na ₂ O	n.d.	0.52	0.37	0.11
TiO ₂	n.d.	<0.01	0.12	0.02
FeO	2.4*	<0.01	0.03	0.28
Cl	12.7	13.5	13.6	12.7

Table 1. Allende wadalite compositions. Ref: terrestrial skarns, wdl-1, 2 and 3: Allende AJEF (*as Fe₂O₃).

References: [1] Kanazawa Y. et al. (1997) *Bull. Geol. Surv. Jpn.*, 48, 413-420.

Acknowledgements: We thank Herbert Palme for providing CAI AJEF used in this study. Portions of this work were performed under the auspices of the U.S. DOE by Lawrence Livermore National Laboratory in part under contract No. W-7405-Eng-48 and in part under contract DE-AC52-07NA27344. This work was supported by NASA Grants NAG5-11591 to KK and NNH06AF991 JPB. QZY acknowledges support of UEPP B556868 grant from LLNL and NASA Grants NNG05GGN22G and NNG05GN03G.